Far-infrared observations of compact objects in nodding and scan mode with ISOPHOT

Attila Moór, Péter Ábrahám, Csaba Kiss, Szilárd Csizmadia

Konkoly Observatory, Budapest, Hungary
25-June-2005

Version 1.0

Contents

1 Introduction and General Principles

The release of the final version of the ISOPHOT Off-Line Processing software (OLP V10.0) and the generation of the ISO Legacy Archive closed the main period of ISOPHOT calibration in 2002. In this phase the calibration work focused on general instrumental effects with impact on several or all observing modes, and the correction algorithms developed were as general as possible in order to ease the software implementation. The photometric quality reached with the OLP is documented in the Scientific Validation Report Richards & Klaas (2002) and in the ISOPHOT Calibration Accuracies Document Klaas et al. (2002).

In a very general calibration approach, however, specific problems of individual observing modes (or submodes) might be overlooked or ignored. In order to improve further the photometric accuracy of ISOPHOT our strategy is to carry out more specific calibration investigations focusing on particular problems of well-defined homogeneous data sets, and to work out dedicated correction algorithms which are not necessarily applicable to other data sets. We adopt the following general scheme for the analysis of a selected well-defined ISOPHOT observing mode or submode:

1. Collect from the Archive all observations performed in the selected observing mode;
2. Identify all objects which can be used as secondary photometric standards;
3. Process the measurements of identified standard objects using an OLP V10.0-compatible data reduction method;
4. Search for any systematic trend in the distribution of the [Measured-Predicted] residual flux densities;
5. Investigate the physical reason behind the observed trend, invent new data processing methods to eliminate it and reprocess the data with the new methods;
6. Repeat Points 4-5 until all understandable physical reasons are eliminated;
7. In case a residual trend is still present in the data, fit the trend and invent an empirical formula to correct for the systematic discrepancies;
8. Document the new processing methods and the empirical fits;

Using this general scheme, in our earlier works we re-evaluated nearly all ISOPHOT observations obtained in the C100/C200 mini-map mode. For a discussion of the special features and advantages of this observing mode see our report "Far-infrared observations of normal stars measured with ISOPHOT in mini-map mode" (Moór et al. (2003); hereafter Report I). In Report I we described the re-evaluation of the mini-map mode as well. We compiled four catalogues including recalibrated fluxes of 1599 measurements of 663 compact objects. These catalogues are available as Highly Processed Data Products (HPDP) in the ISO Data Archive.

The recalibration of C100/C200 nodding and 1D scan measurements is natural extension of our work on mini-maps. By reprocessing these observations we derived new photometric data on point-like or compact sources. The current report documents this project by (i) describing the scan and nodding modes and providing a statistics in the Archive (Sect. 2); (ii) reviewing our new processing scheme (Sect. 3); (iii) discussing special cases (Sect. 4); (iv) presenting an error budget (Sect. 5). Our photometric results are summarized in a catalogue which is described in the Appendix.

2 The ISOPHOT nodding and scan modes

2.1 Definition of the scan observing mode

Typical scans were one-dimensional rasters (DN $= 0''$) of 3 or more points with the source at the centre position. Figure 1 presents a frequently used configuration of a 3x1 C100 and a C200 scan measurement. The figure also outlines the position of the source (second raster step).

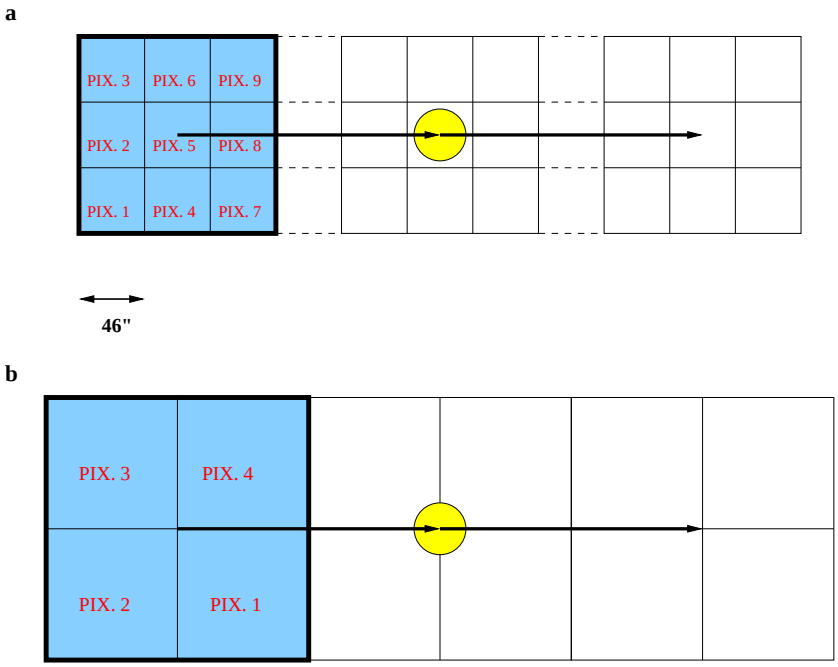

Figure 1: a/ Schematic view of a typical C100 detector scan (3×1 raster steps). Raster steps are indicated by arrows. The target is marked by a yellow circle. b/ Schematic view of a typical C200 detector scan (3×1 raster steps)

2.2 Definition of the nodding observing mode

Nodding measurements were one-dimensional rasters of typically 3 points with the source at the centre but the raster points were scanned several times back and forth to enable elimination of baseline drift ($N \geq 2$, where N is the number of repetition). Figure 2 displays the operation of a typical nodding measurement.

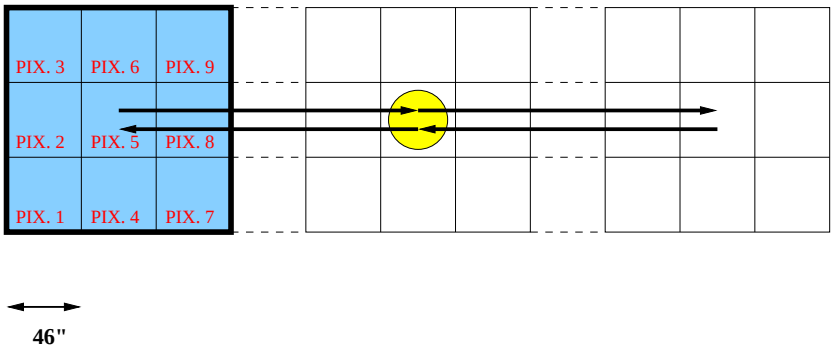

Figure 2: Schematic view of a typical C100 detector nodding observation (3×2 raster steps). Raster steps are indicated by arrows. The target is marked by a yellow circle

2.3 Comparison with other observing modes

In terms of quality the scan/nodding oservations stand halfway between the mini-map mode (the best way of ISOPHOT for point source photometry) and the on/off observing mode. The main differences are listed in the following:

- With the C100 camera in mini-map mode all detector pixels observed the source while in scan and nodding only 1-3 pixels saw it depending on the raster step size (in the typical case only one pixel, Pix. 5). This fact resulted in reduced signal to noise, therefore in a typical case the photometric uncertainty is higher than in mini-maps by a factor of $\sqrt{9} = 3$. Moreover the performance of the C100 pixels were different and Pix. 5 was only of modest quality.
- In nodding and scan observations with C200 camera generally the source was placed on the centre of the array. Thus all four pixels detected the source, but only at the pixel corner resulting in decreased signal to noise. In this respect scan and nodding takes after on/off mode.
- Advantage of scan and nodding mode over the on/off is that we performed a differential measurement, ie. both the background and source positions were observed with the same electronic setup and the detector was active during the whole measurement sequence.
- Like in mini-maps, long term drift can be corrected from the data stream. This is especially true for the nodding where the same spatial positions were observed several times.

2.4 Collecting scan and nodding measurements from the ISO Data Archive

According to our general scheme in the first step we collected all nodding and scan measurements by searching the ISO Data Archive (IDA) for observations using the following criteria:

- Observations performed with the C100 or C200 far-infrared detector were selected;
- AOT P22 or P99 rasters were selected with raster step numbers of $3 \leq \mathrm{M} \leq 7$ and $\mathrm{N} = 1$ (in the case of scan measurements) or $\mathrm{N} \geq 2$ (in the case of nodding measurements). This selection excluded long scans which usually aim at mapping of larger areas and do not center on any compact object;
- the raster step sizes were limited to $\mathrm{DM} \geq 20''$ and $\mathrm{DN} = 0''$

This search in the IDA resulted in 178 TDT numbers including 270 measurements: 21 nodding observations (28 measurements) and 157 scan observations (242 measurements). These observations were further classified into several tentative categories (normal stars, extragalactic objects, young stellar objects, ...) according to keywords from the original proposals and checking SIMBAD. We note that several sparse map sequences (AOT P37/38/39) are similar to our scan and nodding observations in many respects but they are analysed in a separate investigation dedicated to sparse maps (see Csizmadia et al. (2005)).

2.5 Identifying secondary photometric standards

As a second step we selected from this database those objects which can be used as primary or secondary standards in the calibration. These objects can be sorted into three different groups:

1. Stars with photospheric templates produced by M. Cohen and P. Hammersley (primary standards). Five measurements with C100 detector array, and five ones with C200 were found.
2. Normal stars with $B - V < 1.3$. For these objects the photospheric flux densities can be predicted from their K- or V-magnitudes (for details see Report I). Five measurements with C100 detector array, and three ones with C200 were found.

3. Objects for which IRAS photometric data are available. Ten measurements with C100 detector array were found.

According to our general scheme the scan and nodding observing modes should have been calibrated with standard stars measured in these modes. The number of standards found, however, was not enough, therefore we were forced to follow a different strategy: we calibrated the individual pixels using the correction developed for mini-maps, and then validate the adopted calibration using the standards available in scan and nodding mode.

3 Processing scheme

3.1 ERD→AAP processing with PIA v10.0

From the ERD to the AAP level the data were processed in batch mode with the PHOT Interactive Analysis software V10.0 (Gabriel et al. (1997)).

Applied calibration and processing steps	**C100**	**C200**
ERD		
Ramp Linearization	+	+
Ramp Deglitching (2threshold method)	+	+
SRD		
Reset Interval Correction	+	+
Dynamic Transient Correction (external IDL code!)	+	-
Dark Current Subtraction (orbit dependent)	+	+
Signal Linearization	+	+
Signal Deglitching	+	+
Drift recognition	-	+
Correction for long-term drift (external IDL code!)	+	+
Combine signals (SRD → SCP)	+	+
(bi-weight mean averaging method)	+	+
SCP		
Calculate responsivities	+	+
(used the average of the two FCS measurements)		
Convert signals to monochromatic flux	+	+
densities per pixel per raster position		
AAP		

Table 1: Applied calibration and processing steps for the C100 and C200 nodding and scan observations at the different processing levels of PIA V10

Table 1 outlines steps at the subsequent processing levels. Our processing differs from a standard reduction in the following steps:

1. We applied the new dynamic transient correction developed in a joint project of the ISOPHOT Data Centre at MPIA and the Konkoly Observatory. The new transient correction algorithm, not implemented in PIA V10, was available as a separate IDL code. This new method fits the temporal signal evolution within a measurement by interpolating within a library of signal dependent transient curves and predicts the signal at t = 128s (for details see del Burgo et al. (2002)). The transient correction was applied after the reset interval correction at the SRD level. Sometimes, however, this algorithm obviously failed; in these cases, and also for the C200 measurements the PIA drift recognition procedure was used.

2. Scan and nodding measurements last typically 200-400 sec, and on this timescale slow baseline variations, called 'long term drift' may not be negligible. The drift is usually positive, i.e. the signal increases with time even in the case of constant illumination.

   The drift introduces some uncertainty in the estimate of the background signal, and the magnitude of the effect depends on the pixel number (for more details see Report I). In order to correct for artifacts related to drift we used the same method as in the case of reduction of mini-map observations (see Report I), but we performed this correction at the SRD level. In mini-maps the correction was done at the AAP level but at SRD there is better time resolution to characterize the drift curve. Figures 3 and 4 show examples for the drift correction.

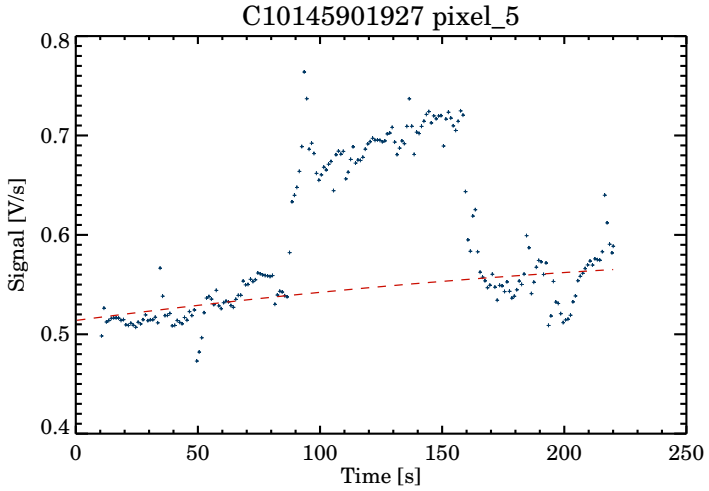

Figure 3: Example of the performance of the drift correction algorithm: original data before correction. Dashed line marks the fitted baseline.

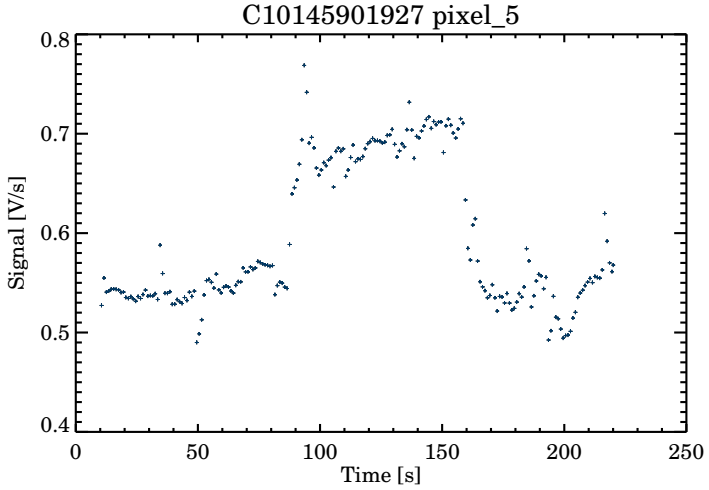

Figure 4: Example of the performance of the drift correction algorithm: corrected data

3. We used the biweight mean method (implemented as a general option in PIA V10.0, which can be used instead of the default weighted mean method) to combine the signals at SRD level because of its beneficial

characteristics.

Since each observation is bracketed by two FCS measurements, there are several possibilities how to combine the two responsivity values. We used the averaging method to calculate the responsivities (it is the default method in PIA V10.0). Of course in those cases where we had only one FCS measurement we used the actual responsivity value.

3.2 Flux extraction from the AAP

Unlike in mini-map mode in nodding and scan measurements not every detector pixel observes the source and the number of background positions may also be limited. For example in standard C100 nodding and scan observations only pixel #5 was illuminated by the source at the centre of the raster (see Fig 1, Fig 2). Due to these facts our standard flux extraction method of PSF fitting could not be used generally, but only in the following cases:

1. C100 observations, where at least two pixels saw the source (for instance: scan measurements with raster step size of 46", where pixel #2, #5 and #8 saw the source);
2. C100 observations, where only one pixel saw the source, but the raster step number was greater than 3 (for instance: typical nodding observations);
3. C200 observations;

For the rest of observations we developed a different flux extraction method where a flat-field correction was also involved. In the following we describe both methods and compare their advantages and disadvantages.

3.2.1 Flux extraction in "mini-map mode", without flat-fielding

In order to extract fluxes from AAP files we normally use a modified version of the PCASPHT method (Kiss & Klaas (2000)). This method is based on the determination of fluxes from the data stream (of each individual pixel). Each pixel at each raster position detects a certain amount of the flux of the (point) source, plus the background assumed to be constant at all positions:

$$I_{ij} = f_{ij} \times I_j^S + I_j^{BG}$$

Here I_j^S is the total flux of the source measured by the jth pixel, I_j^{BG} is the constant background flux, measured by the jth pixel, f_{ij} is the fraction of the source flux on the jth pixel at the ith raster position and I_{ij} is the measured flux on the jth pixel at the ith raster position.

When the source position is known, the f_{ij} values can be derived from the measured beam profiles. As I_{ij}-s are the measured fluxes themselves, there are only two parameters to determine, I_j^S and I_j^{BG} for the jth pixel, which can be done by a simple line-fit using the f_{ij}-s and I_{ij}-s.

3.2.2 Flux extraction with flat-fielding

For those C100 scan maps, which contained only three raster points and the source illuminated only one pixel, we used a different processing scheme. As a first step a flat field array was calculated - using measurements on background raster positions - by normalizing fluxes to the pixel illuminated by the source. After flat-field correction was applied, the source flux can be extracted from the data stream of the second raster position using the method described above.

3.2.3 Comparison of the two methods

Due to different characteristics and time constants of the ISOPHOT pixels (especially in the case of the C100 camera) the flat-fielding procedure in most cases introduces additional noise. Therefore when possible we prefer extracting fluxes from the data streams of individual detector pixels. However, in small scans when only two background positions were observed better estimate of the photometric uncertainty could be achieved by using the flat-field method and computing uncertainty from the 8 border pixels of the C100 detector array. This was not possible for typical C200 scans (at the middle position all four pixels see the source) therefore we always used the "mini-map" like method. Flat-fielding had advantages when the background level change significantly over the spatial extent of the scan, because off position measured with pixel #5 could not provide good background estimate.

3.2.4 Combine photometric results of individual pixels

If more than one pixel was illuminated by the source we averaged their photometric results. Uncertainties were computed from the dispersion of the individual results. In estimating the background we used all pixels.

3.3 Empirical correction for systematic trends

As we concluded in Sect. 2.5 the number of standard objects in nodding and scan mode is not sufficient to recalibrate. In the re-evaluation of mini-maps (see Report I), however, we found that empirical offset and multiplicative corrections were necessary to introduce at the end of the processing scheme. Since nodding and scan mode is very similar intrinsically to mini-maps, in the following we assume that similar empirical correction would be needed in scan and nodding modes, too.

When the point-source flux was extracted in a mini-map like manner (Sect. 3.2.1) then the empirical correction function developed for individual pixels of mini-maps was applied (for details see Report I). In those cases, where the flux extraction was performed with flat fielding (Sect. 3.2.2) then new empirical corrections had to be derived. We simulated this flux reconstruction mode by extracting an appropiate section from each mini-map (utilizing the complete mini-map database of normal stars). Then we determined empirical correction which is of additive nature at low flux level and of multiplicative nature at high flux level. The order of magnitude of the correction in all cases was relatively small: the offset correction was less than 25mJy at all wavelengths and the multiplicative factors varied between 0.91 and 1.1.

4 Individual cases

4.1 Positional issues

In the flux extraction procedure we generally assumed that the source was located at the centre of the raster. In some cases, however, the distribution of signal over the camera pixels were inconsistent with this assumption. Table 2 lists these observations. In the further processing the positional information was taken from external catalogues.

4.2 Other issues

TDT:78100974 The observation of IRAS 00344-3349 was interrupted after the second raster step. Due to this fact only two pixels (Pix. 1 and Pix. 4) observed the source and its data stream contains only two points. Therefore we had to deviate from our general scheme and we extracted flux using the following steps: 1) the photometric results of individual pixels (each data stream contains one off-source and one on-source observation) were derived; 2) empirical correction for the given pixels was applied ; 3) final flux density value was calculated as the average of the two fluxes.

TDT number	Identification	Pos. reference
70603940	LEDA 140899	SIMBAD
71900542	IRAS F19420-1450	IRAS FSC
71900543	IRAS F19420-1450	IRAS FSC
71900739	LEDA 64665	SIMBAD
71900842	LEDA 65116	SIMBAD
83201453	IRAS F04215+2258	IRAS FSC
84000258	LEDA 166501	SIMBAD
84404208	LEDA 1961582	SIMBAD

Table 2: Positional issues

5 Error budget, validation

Although the number of standard object in nodding and scan mode turned out to be insufficient to calibrate these modes (Sect. 2.5) nevertheless they could be used to validate the final photometry, especially the bright flux range of the C100 detector. For the purpose of validation we collected those objects from our database where flux estimate was available (see Sect. 2.5). Color correction was applied except IRAS observations of extragalactic sources where we assumed the effect of color correction to be negligible. Figs. 5 and 6 compare the measured and predicted fluxes. From the figures we concluded that our final photometry did not show any obvious artificial trend.

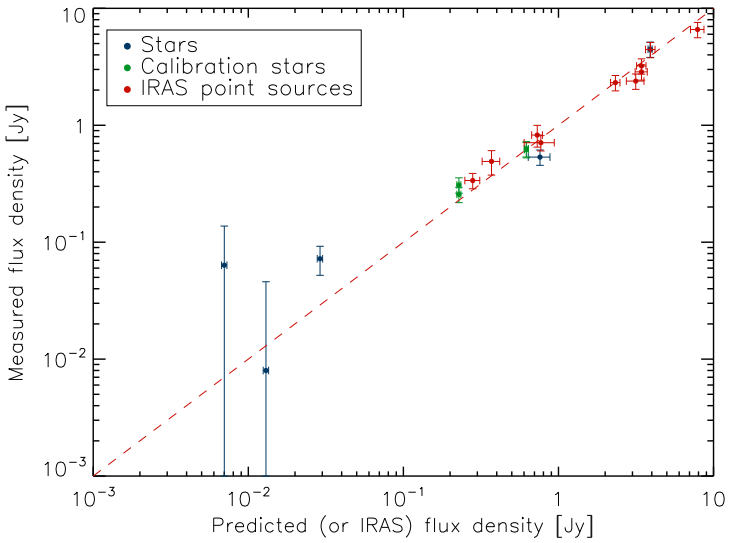

Figure 5: Comparison of measured and predicted (or IRAS) fluxes for 20 measurements with C100 array. Red dashed line corresponding to equal flux are provided to guide the eye and not represent any kind of fitting.

Our processing provides a measurement uncertainty for each data point. However, the comparison of the predicted and measured fluxes suggested that at high flux level the individual error bars were in some cases too low. In order to be on the safe side we decided to modify these individual errors. At high fluxes we requested the flux uncertainty never be lower than the average residual error, 12%. In Figure 5 we plotted these modified error bars. For the faint end of the C100 flux distribution and for the whole C200 range this approach was not possible due to the lack of standard objects. Here we compared our individual errors with the typical uncertainties derived for the mini-maps taking into account the differences between the mini-map and the nodding/scan observing modes. These comparison proved that our individual error bars are realistic in average at low flux level. For bright source

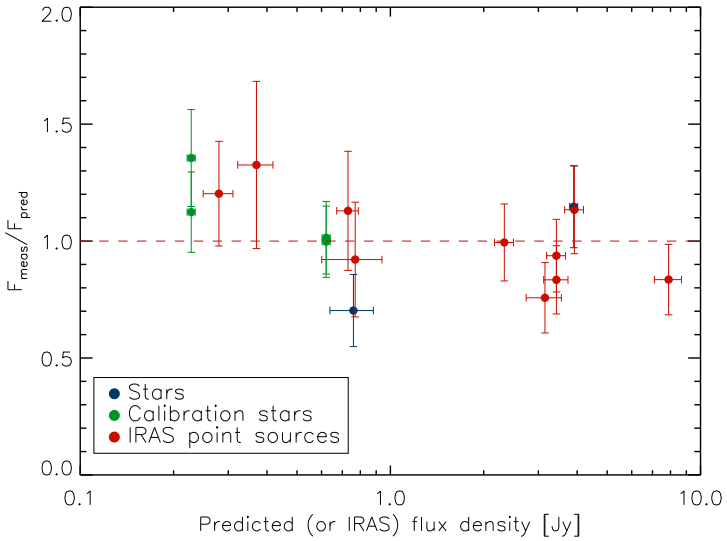

Figure 6: $\mathrm{F_{meas}/F_{pred}}$ flux ratio vs. predicted fluxes. Red dashed line corresponding to equal flux are provided to guide the eye and not represent any kind of fitting.

observations with the C200, however, again we increased the error bars similarly to the method described in the case of C100 measurements.

The typical final photometric uncertainties we derived for scan/nodding observations are the followings: (1) for C100 observation ($60 - 105\mu$m) of bright sources ($\mathrm{F}_\nu > 0.5$Jy) $\sigma \sim 12\%$; (2) for C100 observation of faint sources ($\mathrm{F}_\nu < 0.2$Jy) $\sigma = 45\,$mJy; (3) for C200 observation ($105 - 200\mu$m) of bright sources ($\mathrm{F}_\nu > 1.0$Jy) $\sigma \sim 11\%$; (4) for C200 observation of faint sources ($\mathrm{F}_\nu < 0.5$Jy) $\sigma = 70\,$mJy;

The individual errors however may spread in larger range. In some special nodding configurations the drift was very efficiently cancelled and photometric accuracy was comparable that of the mini-maps in the $\sim 15 - 20\,$mJy.

References

Csizmadia, Sz., Ábrahám, P., Moór, A., Kiss, Cs., 2005, Far-infrared observations of normal stars measured with ISOPHOT C100/C200 in sparse map mode

del Burgo, C. et al., Proceedings of the Conference Exploiting the ISO Data Archive. Infrared Astronomy in the Internet Age, in Siguenza, Spain 24-27 June, 2002. Edited by C. Gry et al. To be published as ESA Publications Series, ESA SP-511

Gabriel C., 1997, in Proc. of the ADASS VI conference (Eds.: G. Hunt, H.E. Payne, ASP Conf.Ser. 125), 108

Jayawardhana, R. et al., 2002, ApJ, 570, L93

Kiss, Cs., Klaas, U., 2000, "General Re-validation of Point Source Photometry from PHT22 Mini-Maps"

Richards, P., Klaas, U., "Report on the Scientific Validation of the mini-map photometry processing in the PHT pipeline (Version 1.0)"

Klaas U. et al., 2002, "ISOPHOT Calibration Accuracies (Version 5.0)"

Moór, A., Ábrahám, P., Kiss, Cs., Csizmadia, Sz., 2003, Far-infrared observations of normal stars measured with ISOPHOT in mini-map mode (http://pma.iso.vilspa.esa.es:8080/hpdp/techn ical_reports/technote5.pdf)

6 Appendix: description of the catalogue

The flux densities for scan and nodding measurements resulted from recalibration described in this document were listed in a photometric catalogue which is included as Highly Processed Data Product. In the following we described the fields of the catalogue. We note that observations of young stellar objects were taken out from this list and will be included in a separate catalogue. In addition there were a few observations excluded from the catalogue due to different technical reasons.

Column	Field	Unit	Format	Description
(1)	Object name			SIMBAD compatible name or target name as given by the original ISO proposer
(2)	Object type			Standard SIMBAD code for object type
(3)	ISO name			Object name given by the ISO observer
(4)	TDTNUM_ON			The 8-digit TDTNUM of the on-source observation
(5)	On_ Meas.			Index of the on-source measurement within TDTNUM_ ON
(6)	RA(2000)			Right ascension, h:m:s
(7)	Dec(2000)			Declination, d:m:s
(8)	Detector			ISOPHOT detector (P1, P2, P3, C100, or C200)
(9)	Wavelength	[micron]		Nominal wavelength of the ISOPHOT filter
(10)	Aperture	[arcsec]		Circular for P1,P2,P3, square for C100 and C200 detectors
(11)	Epoch			Epoch of the observation
(12)	TDTNUM_ OFF			The 8-digit TDTNUM of the off-source observation
(13)	Off_Meas.			Index of the off-source measurement within TDTNUM_OFF
(14)	Flux density	[Jy]		Flux density of the source. In case of a point source the measured flux is corrected for the size of the point spread function. In case of an extended source it corresponds to the integrated brightness. No colour correction applied.
(15)	Flux uncertainty	[Jy]		Flux uncertainty. No colour correction applied.
(16)	Background	[MJy/sr]		Background surface brightness. No colour correction applied.
(17)	Detection	[sigma]		The significance level of the source being detected above the background. -99 marks those case where no useful value could be defined
(18)	Object size			Indicates if the object is point-like (P) or extended (E)
(19)	Quality			Quality of the observation R1 – Standard processing according to the scheme described in the report. R2 – Minimap performed in astronomical (rather than satellite) coordinate R3 – ISOPHOT position differs from SIMBAD position by more than 10” R4 – Suspected ISO pointing problem R5 – Only one FCS is available R6 – No useful FCS is available, default FCS is used R7 – Archive quality mark R8 – Not enough data points to perform drift correction R9 – Fitting smooth baseline to the data points failed, drift correction (partly/completely) omitted R10 – Observation was carried out at the very end of orbit. Reduced photometric reliability at orbital phase greater than 0.8 R11 – A large increase in the proton flux from the Sun was observed R12 – Non-stabilised target signal R13 – Measured flux was out of the empirically calibrated range

Table 3: Description of the catalogue